International Journal of Scientific Research in Mathematical and Statistical Sciences
Vol.**11**, Issue.**6**, pp.**47-59**, December **2024**
E-ISSN: 2348-4519
Available online at: www.isroset.org

Research Article

Mathematical Analysis of Fractional Burgers' Fluid Model of Magnetohydrodynamic Blood Flow through Bifurcated Arteries

Isah Abdullahi[1*], M.Y Adamu[2], A. M Kwami[3], Munira Salisu[4]

[1,2,3]Dept. of Mathematics, Abubakar Tafawa Balewa University, Bauchi, Nigeria
[4]Dept. of Mathematics, University of Maiduguri, Borno State Nigeria

**Corresponding Author isaabdullahi7474@gmail.com*

Received: 16/Oct/2024; **Accepted**: 20/Nov/2024; **Published**: 31/Dec/2024

Abstract— The study analyzes electro-magnetohydrodynamic (EMHD) flow in bifurcated arteries using a non-Newtonian Burgers' fluid model with an Atangana-Baleanu fractional derivative. The focus is on how magnetic fields, electric fields, and thermal properties affect blood flow, especially for enhancing tumor treatment via controlled heat transfer. The study formulates the nonlinear partial differential equations (momentum, energy, and concentration) and solved analytically using the combine Laplace transforms and the Homotopy Perturbation Method (HPM). The results show that parameters such as magnetic field strength, Burgers' parameter, fractional parameters, Eckert number, and Joule heating influence blood flow velocity, temperature, and concentration within the arteries. Specifically, stronger magnetic fields and higher Burgers' parameters reduce blood velocity, while thermal factors like Eckert number and Joule heating increase temperature. These insights are valuable for biomedical applications such as targeted drug delivery, heat management, and tumor therapy.

Keywords— Bifurcated artery, Burgers' fluid model, Atangana-Baleanu Fractional time derivative, Magnetic field, Thermal radiation, Heat transfer

1. Introduction

In the study of fluid dynamics in biological systems, particularly blood flow in arteries, understanding the behavior of fluids is essential for addressing both physiological and pathological conditions. Blood's non-Newtonian, viscoelastic nature can be accurately modeled using the Burgers' fluid model, which has been widely explored in various contexts. For instance, Hayat et al. [1] examined the peristaltic flow of Burgers' fluid in a porous medium, focusing on heat and mass transfer, and provided analytical solutions for the velocity, temperature, and concentration profiles. Similarly, Khan and Shahzadi [2] studied the MHD flow of Burgers' fluid over a stretching sheet, emphasizing the effects of heat transfer and using similarity transformations to numerically solve the governing equations, particularly looking at the influence of magnetic fields and heat transfer on fluid behavior. Hayat et al. [3] also analyzed oscillatory flow in a porous medium under magnetic fields and thermal radiation, applying the Laplace transform method to obtain exact solutions for the velocity and temperature fields. Additionally, Yakubu et al. [4] explored the unsteady flow of Burgers' fluid in a cylindrical tube, incorporating factors such as a time-varying pressure gradient, body acceleration, and magnetic fields to examine their effects on blood velocity and temperature.

Research on fractional calculus has grown significantly, particularly with the advent of the Atangana-Baleanu fractional derivatives, introduced by Atangana and Baleanu in 2016 [6]. Their groundbreaking work, "New Fractional Derivatives with Non-Local and Non-Singular Kernel: Theory and Application to Heat Transfer Model," provided a theoretical framework and demonstrated applications in heat transfer, sparking further interest in the field. Smith and Johnson [7] applied these derivatives to control systems, highlighting their effectiveness in designing controllers for fractional-order dynamics. Meanwhile, Chen and Wang [8] focused on analytical solutions for fractional differential equations in viscoelasticity, advancing material modeling in engineering.

2. Related Work

In the context of non-Newtonian fluid modeling, Mirza et al. [9] investigated the effects of magnetic fields on blood flow in stenosed arteries, including wall-slip conditions, showing that the Lorentz force reduced both velocity and shear stress in magnetically conducting blood. Kumar et al. [10] explored the impact of heat sources and chemical reactions on MHD blood flow in permeable bifurcated arteries under an inclined magnetic field, with a focus on tumor treatment, demonstrating the potential for improving drug delivery and

managing high blood pressure. Isah et al. [11] examined the combined effects of electric and magnetic fields on MHD blood flow in permeable bifurcated arteries using a Newtonian fluid model, revealing key insights into the interaction of electromagnetic fields and heat radiation for clinical blood flow management.

Previous studies have mostly focused on simplified models, neglecting the combined effects of magnetic fields, thermal radiation, and viscoelastic properties. Therefore, developing comprehensive models that integrate Burgers' fluid's viscoelastic properties, fractional time derivatives, magnetic fields, and thermal radiation within bifurcated arteries is crucial for advancing our understanding of complex blood flow, especially for applications in tumor treatment. This research aims to analytically solve such models, providing exact solutions to capture the interaction of these factors and offering insights into blood flow dynamics in medical treatments.

3. Theory/Calculation

Definition1 $Let\ u \in H^1(a,b), a < b, \propto \in [0,1]$. Then the Atangana-Baleanu fractional derivative is defined as follows: left and right derivatives in Caputo sense;

$$ {}^{ABC}D_t^{\alpha}u(t) = \frac{N(\alpha)}{1-\alpha}\int_a^t E_{\alpha}\left(\frac{-\alpha(t-s)^{\alpha}}{1-\alpha}\right)u'(s)ds.$$

$$ {}^{ABC}D_t^{\alpha}u(t) = \frac{-N(\alpha)}{1-\alpha}\int_t^b E_{\alpha}\left(\frac{-\alpha(s-t)^{\alpha}}{1-\alpha}\right)u'(s)ds. \quad (1)$$

where $N(\alpha) > 0$ is a normalization function satisfying $N(0) = N(1) = 1$, and E_{α} is the well-Known Mittag–Leffler function of one variable defined by

$$E_{\alpha}(z) = \sum_{k=0}^{\infty}\frac{z^k}{\Gamma(\alpha k+1)}, z\ \epsilon, \mathbb{C}\ \Re e(\propto) > 0) \quad (2)$$

Definition 2. The Laplace transform of Atangana-Baleanu time-fractional derivative of equation (1) is defined by Atangana-Baleanu. (2016) as:

$$L\{{}^{AB}D_t^{\alpha}u(t)\}s = \frac{N(\alpha)}{1-\alpha}\frac{s^{\alpha}L\{u(t)\}s - s^{\alpha-1}u(0)}{s^{\alpha}+\frac{\alpha}{1-\alpha}} \quad (3)$$

Definition 3. The Inverse Laplace transform of some special functions have the following properties:

$$\left.\begin{aligned} L^{-1}\left\{\frac{a}{s^{\alpha}-a}\right\} &= E_{\alpha}(at^{\alpha}), \left|\frac{a}{s^{\alpha}}\right|. < 1 \\ L^{-1}\left\{\frac{s^{\alpha-1}}{s^{\alpha}-\mu_{\alpha}}\right\} &= E_{\alpha}(-\mu_{\alpha}t^{\alpha}), \ \left|\frac{\mu_{\alpha}}{s^{\alpha}}\right|. < 1 \end{aligned}\right\} \quad (4)$$

3.1 Problem Formulation

In the mathematical analysis of fluid dynamics, foundational assumptions are essential to model blood flow accurately within the circulatory system. Blood is considered a non-Newtonian fluid, displaying compressibility, homogeneity, and viscosity, which moves through a parallel-plate, non-conducting channel from the central artery trunk to branching arteries. The mass flow rate, determined at any cross-sectional area perpendicular to the flow direction, is represented by m=2bV, where mmm is the mass flow rate, V is the mean fluid velocity, b represents the vessel's radius or diameter, and ρ is blood density. Due to the relatively small dimensions of the bifurcated wall compared to the overall circulatory system, the mass flow rate is effectively split in half at any cross-sectional plane within each branched channel, as depicted in Figure 1.

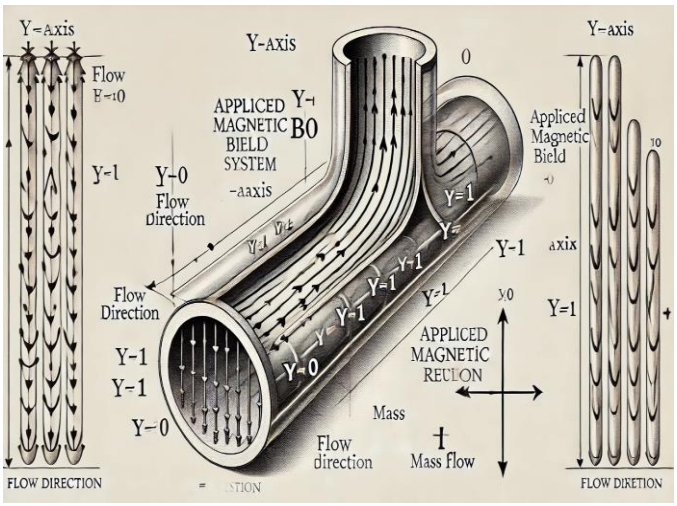

Figure 1: Geometrical structure of bifurcated artery

3.2 Basic flow equations

In the study of fluid flow dynamics, particularly in the context of drug transport for tumor treatment through permeable bifurcated arteries, our focus typically centres on a fundamental group of equations. These equations encompass the momentum equation, the energy equation, the concentration equation, and the continuity equation, all of which are detailed in the research [10,11]

$$\rho\frac{\partial\bar{u}}{\partial\bar{t}} + \frac{\partial\bar{p}}{\partial\bar{x}} = \frac{\partial}{\partial y}\tau_{xy}(y,t) + g\beta(T-T_{\infty}\bar{)} + g\beta'(C-C_{\infty}\bar{)} - \frac{\sigma B_0^2\sin^2\phi}{\rho}\bar{u} - \frac{\bar{u}}{\bar{k}} + \rho_e E_x \quad (5)$$

$$\frac{\partial\bar{\theta}}{\partial\bar{t}} = \frac{k_T}{\rho C_{\rho}}\frac{\partial^2\bar{\theta}}{\partial\bar{y}^2} + \frac{Q}{\rho C_{\rho}}(\theta-\theta_{\infty}\bar{)} - \frac{\partial\bar{q}}{\partial\bar{y}} + \frac{J.J}{\sigma_e} + \tau_{xy}\frac{\partial u}{\partial y} \quad (6)$$

$$\frac{\partial\bar{C}}{\partial\bar{t}} = D\frac{\partial^2\bar{C}}{\partial\bar{y}^2} + G + \frac{DK_T}{T_m}\frac{\partial^2\bar{T}}{\partial\bar{y}^2} \quad (7)$$

$$\frac{\partial \bar{u}}{\partial \bar{x}} + \frac{\partial \bar{v}}{\partial \bar{y}} = 0 \tag{8}$$

where ρ is the fluid density, $\frac{\partial}{\partial t}$ is the material time derivative, ρ_e denote the net charge density of the applied electric field in the blood flow, τ_{xy} the Cauchy stress tensor, E_x is the external electric field imposed at the ends of the arterial bifurcated wall, ρ is the fluid density, C_P is the specific heat capacity of the fluid, T is the temperature, $\vec{j}$ is the current density given by the Ohm's law, σ_e is the electrical conductivity, k_T is the thermal conductivity of the fluid, $\frac{\vec{j}\,\vec{j}}{\sigma_e}$, is the Joule heating effect created by the current density, $\frac{\partial \bar{q}}{\partial \bar{y}}$ is the radiative heat transfer $\bar{u}$ and $\bar{v}$ are the velocity components in the direction of $\bar{x}$ and $\bar{y}$ respectively at time t in the flow field, $G = -k_1(C - C_\infty)$ is any constant (G = 1) and D is the diffusion coefficient, see[10,11,12]. The Cauchy stress tensor, τ_{xy} is defined in [13] is given by:

$$\tau_{xy}(y,t) = \mu \frac{\left(1 + \lambda_2^{\beta} D_t^{\beta}\right)}{\left(1 + \lambda_1^{\alpha} D_t^{\alpha} + \lambda_3^{2\alpha} D_t^{2\alpha}\right)} \frac{\partial}{\partial y} u(y,t). \tag{9}$$

The boundary conditions in consideration are:

$$\left.\begin{aligned} &\theta = \ell^{-\lambda^2 t}, u = \ell^{-\lambda^2 t}, v = \ell^{-\lambda^2 t}, \\ &C = \ell^{-\lambda^2 t}, at \quad y = -1 \\ &\theta \to 0,\ u \to 0,\ v \to 0, \\ &C \to 0, at \quad y = 1 \end{aligned}\right\} \tag{10}$$

3.3 Applied electric field

This section investigates the behaviour of blood flow in a bifurcated artery, where a branch of diameter b, carries a compressible, homogeneous, viscous non-Newtonian fluid. The fluid moves through a parallel-plate, non-conducting channel with a uniform dielectric permittivity, and the bifurcation wall directs the flow from the main trunk into the branches, as shown in Figure 1. Based on these assumptions and using principles from electrostatics, the net charge density ρ_e can be derived via the Poisson equation, consistent with prior studies [10,11,14].

$$\frac{\partial^2 \Phi}{\partial x^2} + \frac{\partial^2 \Phi}{\partial y^2} = -\frac{\rho_e}{\in} \tag{11}$$

In this context, Φ represents the electric potential within the bifurcation wall, and ε is the dielectric permittivity of the fluid. We assume the total electric potential is a linear combination of the externally applied electric potential in the x-direction and the equilibrium electric potential, which holds true for values of Ψ , valid for ($-1 \le y \le 1$).

Therefore, we can write

$$\Phi = \varphi(x) + \psi(y) \tag{12}$$

Focusing on the upper and lower sections of the arterial wall, the primary fluid flow occurs in the y-direction, with velocity in the x-direction being negligible. Substituting (12) into the Poisson equation (11) leads to the result:

$$\frac{d^2\psi}{d\,y^2} = -\frac{\rho_e}{\in} \tag{13}$$

where the net charge density of the blood is given by the Boltzmann distribution:

$$\rho_e = -2z\eta_0 e \sinh\left(\frac{ze\Psi}{k_B T}\right) \tag{14}$$

where z, η_0, e, k_B and T are the valence electron, ion density, fundamental charge, Boltzmann constant and absolute temperature, respectively. Equation (13) subject to the following boundary conditions at the top and bottom of the walls of the artery, are

$$\left.\begin{aligned} &\psi = \xi_1, \quad at \quad y = -1 \\ &\psi = \xi_2 \quad at \quad y = 1 \end{aligned}\right\} \tag{15}$$

$\sinh\left(\frac{ze\Psi}{k_B T}\right) \approx \left(\frac{ze\Psi}{k_B T}\right)$ for $\left(\frac{ze\Psi}{k_B T}\right) << 1$, hence (13) becomes

$$\frac{d^2\psi}{d\,y^2} = k_e^2\,\psi \tag{16}$$

where:

$$\left(\frac{2\eta_0 z^2 e^2}{\in k_B T}\right) = k_e^2$$

is the Debye-Hückel parameter.

The solution of equation (16) subject to the boundary conditions (15) is given by

$$\psi = \xi_1 \left[\begin{aligned} &\ell^{k_e} - \ell^{2k_e}\left(\frac{\ell^{3k_e} - R_\xi \ell^{k_e}}{2Sinh2k_e}\right)\ell^{k_e y} \\ &+ \left(\frac{\ell^{k_e} - R_\xi \ell^{k_e}}{2Sinh2k_e}\right)\ell^{-k_e y} \end{aligned} \right] \tag{17}$$

where:

$$R_{\xi} = \frac{\xi_1}{\xi_2}$$

is the ratio of zeta potential of an applied electric field. From equation (13) and (16) we have:

$$\rho_e = -k_e{}^2 \psi \in \quad (18)$$

Putting (17) into (18) we get

$$\rho_e = - \in k_e{}^2 \xi_1 (A_0 \ell^{k_e y} + B_0 \ell^{-k_e y}) \quad (19)$$

where s

Equation (19), can also be written as:

$$\rho_{e\ =\ -} \in k_e{}^2 \xi_1 \left((A_0 Coshk_e y + B_0 Sinhk_e y) \right) \quad (20)$$

$$\rho_e E_x = -E_x \in k^2 \xi_1 \left(A_0 Coshk_e y + B_0 Sinhk_e y \right) \quad (21)$$

Considering the factors previously discussed, we introduce non-dimensional parameters to streamline our analysis, resulting in the following:

$$\left.\begin{aligned}
&x = \frac{\bar{x}}{b},\ y = \frac{\bar{y}}{b}, u = \frac{\bar{u}}{mu_{HS}/2b\rho}, v = \frac{\bar{v}}{mu_{HS}/2b\rho},\\
&h(x,t) = \frac{d\bar{p}/d\bar{x}}{\eta m u_{HS}/2b^3\rho}, k = \frac{\bar{k}}{\left(\frac{b^2\rho}{\eta}\right)},\\
&C = \frac{\left(\bar{C} - C_w\right)(2b^3\rho^2)}{\left(C_w - C_\infty\right)m\eta u_{HS}}, \mu = \frac{\eta}{\rho}, t = \frac{\bar{t}}{\left(\frac{b^2\rho}{\eta}\right)},\\
&\theta = \frac{\left(\bar{T} - T_w\right)(2b^3\rho^2)}{\left(T_w - T_\infty\right)m\eta u_{HS}} u_{HS} = \frac{-2 \in E_X \xi_1 b\rho^2}{\eta m},\\
&k_e = \bar{k}_e b, \bar{q} = \frac{-16\delta' T_0^3}{3k'}\frac{\partial \bar{T}}{\partial \bar{y}},\\
&\lambda_1 = \frac{\bar{\lambda}_1 \mu}{b^2\rho}, \lambda_2 = \frac{\bar{\lambda}_2 \mu}{b^2\rho}, \lambda_3 = \frac{\bar{\lambda}_3 \mu}{b^2\rho}
\end{aligned}\right\} \quad (22)$$

By applying equation (9), (21) and (22) into equations; 5-8 and dropping the bars, we have:

$$\frac{\partial u}{\partial t} + h = \frac{\left(1 + \lambda_2^\beta D_t^\beta\right)}{\left(1 + \lambda_1^\alpha D_t^\alpha + \lambda_3^{2\alpha} D_t^{2\alpha}\right)} \frac{\partial^2 u}{\partial y^2} + g\beta\theta + g\beta' C - M^2 \sin^2\phi - \frac{u}{K} + g(y) \quad (23)$$

$$\frac{\partial \theta}{\partial t} = \left(\frac{1}{\varpi_r} + R\right)\frac{\partial^2 \theta}{\partial y^2} + \left(\frac{S}{\varpi_r} + \delta_E\right)\theta + JHE_C + Br\left(\frac{\left(1 + \lambda_2^\beta D_t^\beta\right)}{\left(1 + \lambda_1^\alpha D_t^\alpha + \lambda_3^{2\alpha} D_t^{2\alpha}\right)}\right)\left[\frac{\partial u}{\partial y}\right]^2 \quad (24)$$

$$\frac{\partial C}{\partial t} = \frac{1}{S_C}\frac{\partial^2 C}{\partial y^2} - \omega C + Sr\frac{\partial^2 \theta}{\partial y^2} \quad (25)$$

Where

$$g(y) = A\cosh(k_e y) + B\sinh(k_e y),$$
$$A = A_0 k_e^2, \quad and \quad B = B_0 k_e^2.$$

$$\left.\begin{aligned}
&M^2 = \frac{\sigma B_0^2}{\rho}, p_r = \frac{\rho C_\rho}{k_T}, R = \frac{16\delta' T_0^3}{3k'\tau},\\
&S = \frac{Qb^2}{k_T}, JH = \frac{\sigma_e Q B_0^2 u_{HS}}{2\rho\tau^2},\\
&\delta_E = \frac{2\sigma_e C_\rho b^5 E_y^2}{\tau^2}, E_C = \frac{u^2}{C_\rho \theta},\\
&S_C = \frac{\tau}{bD}, Br = \frac{\mu u^2}{k(T_w - T_\infty)},\\
&Sr = \frac{D_m K_T (T_w - T_\infty)}{\tau T_m (C_w - C_\infty)} and \quad \omega = \frac{k_1 b^2}{\tau}
\end{aligned}\right\} \quad (26)$$

M^2 is the magnetic field parameter, Pr is the Prandtl number, R is the Thermal radiation parameter, S is the Heat source, parameter δ_E is the dielectrically constant, JH is the Joule heating parameter, Ec is the Eckert number, S_C is the Schmidt number, Brickman number, Soret Number and ω is the Chemical reaction parameter respectively.

4. Experimental Method/Procedure/Design

A hybrid method was developed to solve the equations governing blood flow and heat transfer. It combines a modified Homotopy Perturbation Method (HPM) that incorporates He's polynomial with the traditional HPM framework and the Laplace transform technique. This section provides an overview of the classical Homotopy Perturbation Method (HPM) by He [15], designed to solve non-linear Ordinary Differential Equations (ODEs). Consider the following differential equation:

$$E(u) = g(r) \quad \ldots (27)$$

with boundary condition:

$$B\left(u, \frac{\partial u}{\partial n}\right) = 0 \quad (28)$$

where $E(u)$ represents any differential operator and B denotes a boundary operator. According to He, the differential operator E(u) is divided into two components: the linear and non-linear parts.

$$L(u) + N(u) = g(r) \quad (29)$$

The Homotopy equation is constructed as:

$$L(u) + pN(u) = g(r) \quad (30)$$

where $p\varepsilon[0,1]$ is an embedding parameter.

First, consider the linear part of equation (30) and express it in a series form:

$$L(u) = L\left[\sum_{i=0}^{\infty} p^i u_i\right] \quad \ldots(31a)$$

which implies that

$$L\left[\sum_{i=0}^{\infty} p^i u_i\right] = pL(u_0) + p^1 L(u_1) + p^2 L(u_2) + \cdots \quad (31b)$$

Next, consider the non-linear part of equation (30) and express it in polynomial form:

$$N(u) = \sum_{i=0}^{\infty} P^n H_n \quad \ldots(32)$$

which implies that

$$N(u) = \sum_{n=0}^{\infty} P^n H_n = H_0 + PH_1 + P^2 H_2 + \cdots \quad \ldots(33)$$

where H_n is the He polynomial defined by

$$H_n = \frac{1}{n!}\frac{d^n}{dp^n} N\left[\sum_{n=0}^{\infty} P^i H_i\right]_{p=0} \qquad n = 0,1,2,\ldots \quad \ldots(34)$$

Now, substituting equations (31a) and (33) into equation (30) and obtain the following:

$$L\left(\sum_{n=0}^{\infty} p^i U_i\right) + \sum_{n=0}^{\infty} p^{i+1} H_i = g(r) \quad \ldots(35)$$

Now, applying equation (1) to equations (23), (24), and (25), we have;

$$\left.\begin{aligned}
&{}^{ABC}D_t^{\alpha} u(t) + h = \frac{\left(1+\lambda_2^{\beta} D_t^{\beta}\right)}{\left(1+\lambda_1^{\alpha} D_t^{\alpha} + \lambda_3^{2\alpha} D_t^{2\alpha}\right)}\frac{\partial^2 u}{\partial y^2} + \\
&g\beta\theta + g\beta' C - M^2 \sin^2\phi - \frac{u}{K} + g(y) \\
&{}^{ABC}D_t^{\alpha}\theta(t) = \left(\frac{1}{\text{Pr}} + R\right)\frac{\partial^2\theta}{\partial y^2} + \left(\frac{S}{\text{Pr}} + \delta_E\right)\theta + \\
&JHE_C + Br\left(\frac{\left(1+\lambda_2^{\beta} D_t^{\beta}\right)}{\left(1+\lambda_1^{\alpha} D_t^{\alpha} + \lambda_3^{2\alpha} D_t^{2\alpha}\right)}\right)\left[\frac{\partial u}{\partial y}\right]^2 \\
&{}^{ABC}D_t^{\alpha} C(t) = \frac{1}{S_C}\frac{\partial^2 C}{\partial y^2} - \omega C + Sr\frac{\partial^2\theta}{\partial y^2}
\end{aligned}\right\} \quad (36)$$

Taking the Laplace transform of (29) and (10) yields

$$\left.\begin{aligned}
&\frac{N(\alpha)}{1-\alpha}\frac{s^{\alpha} L\{u(t)\}s - s^{\alpha-1}u(0)}{s^{\alpha} + \frac{\alpha}{1-\alpha}} + h = \\
&\frac{\left(1+\lambda_2^{\beta} s^{\beta}\right)}{\left(1+\lambda_1^{\alpha} s^{\alpha} + \lambda_3^{2\alpha} s^{2\alpha}\right)}\frac{\partial^2 \bar{u}(y,s)}{\partial y^2} + g\beta\bar{\theta}(y,s) + \\
&g\beta'\bar{C}(y,s) - \\
&M^2 \sin^2\phi\bar{u}(y,s) - \frac{\bar{u}(y,s)}{K} + \frac{g(y)}{s} \\
&\frac{N(\alpha)}{1-\alpha}\frac{s^{\alpha} L\{\theta(t)\}s - s^{\alpha-1}\theta(0)}{s^{\alpha} + \frac{\alpha}{1-\alpha}} = \\
&\left(\frac{1}{\text{Pr}} + R\right)\frac{\partial^2\bar{\theta}(y,s)}{\partial y^2} + \left(\frac{S}{\text{Pr}} + \delta_E\right)\bar{\theta}(y,s) + \\
&\frac{JHEc}{s} + Br\left(\frac{\left(1+\lambda_2^{\beta} s^{\beta}\right)}{\left(1+\lambda_1^{\alpha} s^{\alpha} + \lambda_3^{2\alpha} s^{2\alpha}\right)}\right)\left[\frac{\partial\bar{u}(y,s)}{\partial y}\right]^2 \\
&\frac{N(\alpha)}{1-\alpha}\frac{s^{\alpha} L\{C(t)\}s - s^{\alpha-1}C(0)}{s^{\alpha} + \frac{\alpha}{1-\alpha}} = \\
&\frac{1}{S_C}\frac{\partial^2\bar{C}(y,s)}{\partial y^2} - \omega\bar{C}(y,s) + Sr\frac{\partial^2\bar{\theta}(y,s)}{\partial y^2}
\end{aligned}\right\} \quad (37)$$

$$\left.\begin{aligned}
&\bar{\theta}(y,s) = \frac{1}{s+\lambda^2}, \bar{u}(y,s) = \frac{1}{s+\lambda^2}, \\
&\bar{v}(y,s) = \frac{1}{s+\lambda^2}, \bar{C} = \frac{1}{s+\lambda^2} \\
&at \qquad y = -1 \\
&\theta \to 0,\ u \to 0,\ v \to 0, \\
&C \to 0 \ \ at \qquad y = 1
\end{aligned}\right\} \quad (38)$$

Where $N(\alpha) > 0$ is a normalization function satisfying $N(0) = N(1) = 1,\ u(0) = \theta(0) = C(0) = 0$.

Now, after rearranging equation (37), we obtain:

$$\left.\begin{aligned}
&\left(1+\lambda_2^{\beta}s^{\beta}\right)\frac{\partial^2\bar{u}}{\partial y^2}-\Lambda\bar{u}(y,s)\\
&-\frac{h}{s}+\delta\bar{\theta}(y,s)+\gamma\bar{C}(y,s)+\frac{g(y)}{s}=0\\
&K_1\frac{\partial^2\bar{\theta}(y,s)}{\partial y^2}-\eta\bar{\theta}(y,s)+\\
&\frac{JHEc}{s}+Br\left(1+\lambda_2^{\beta}s^{\beta}\right)\left[\frac{\partial\bar{u}(y,s)}{\partial y}\right]^2=0\\
&\frac{\partial^2\bar{C}(y,s)}{\partial y^2}-\zeta\bar{C}(y,s)+SrSc\frac{\partial^2\bar{\theta}(y,s)}{\partial y^2}=0
\end{aligned}\right\} \quad (39)$$

4.1 Solution Procedure using HPM

Using the method known as the HPM procedure, we formulate the following Homotopy in the manner described below:

$$H_1(u,p):\phi\times[0,1]\to\Re$$
$$H_2(u,p):\nu\times[0,1]\to\Re$$
$$H_3(u,p):\omega\times[0,1]\to\Re$$

The above can now be represented as the following expression.

$$\left.\begin{aligned}
&H_1(u,p)=(1-p)\left(\frac{\partial^2 u}{\partial y^2}-\frac{\partial^2 u_0}{\partial y^2}\right)+\\
&p\left(\begin{aligned}&\left(1+\lambda_2^{\beta}s^{\beta}\right)\frac{\partial^2\bar{u}}{\partial y^2}-\Lambda\bar{u}(y,s)\\&-\frac{h}{s}+\delta\bar{\theta}(y,s)+\gamma\bar{C}(y,s)+\frac{g(y)}{s}\end{aligned}\right)\\
&H_2(u,p)=(1-p)\left(\frac{\partial^2\theta}{\partial y^2}-\frac{\partial^2\theta_0}{\partial y^2}\right)+\\
&p\left(\begin{aligned}&K_1\frac{\partial^2\bar{\theta}(y,s)}{\partial y^2}-\eta\bar{\theta}(y,s)+\\&\frac{JHEc}{s}+Br\left(1+\lambda_2^{\beta}s^{\beta}\right)\left[\frac{\partial\bar{u}(y,s)}{\partial y}\right]^2\end{aligned}\right)\\
&H_3(u,p)=(1-p)\left(\frac{\partial^2 C}{\partial y^2}-\frac{\partial^2 C_0}{\partial y^2}\right)+\\
&p\left(\frac{\partial^2\bar{C}(y,s)}{\partial y^2}-\zeta\bar{C}(y,s)+SrSc\frac{\partial^2\bar{\theta}(y,s)}{\partial y^2}\right)
\end{aligned}\right\} \quad (40)$$

By letting $H_1(u,p)=H_2(u,p)=H_3(u,p)=0$,

We obtain equivalent equations in the following form:

$$\left.\begin{aligned}
&(1-p)\left(\frac{\partial^2 u}{\partial y^2}-\frac{\partial^2 u_0}{\partial y^2}\right)+\\
&p\left(\begin{aligned}&\left(1+\lambda_2^{\beta}s^{\beta}\right)\frac{\partial^2\bar{u}}{\partial y^2}-\\&\Lambda\bar{u}(y,s)-\frac{h}{s}+\delta\bar{\theta}(y,s)+\gamma\bar{C}(y,s)+\frac{g(y)}{s}\end{aligned}\right)=0\\
&(1-p)\left(\frac{\partial^2\theta}{\partial y^2}-\frac{\partial^2\theta_0}{\partial y^2}\right)+\\
&p\left(\begin{aligned}&K_1\frac{\partial^2\bar{\theta}(y,s)}{\partial y^2}-\eta\bar{\theta}(y,s)+\\&\frac{JHEc}{s}+Br\left(1+\lambda_2^{\beta}s^{\beta}\right)\left[\frac{\partial\bar{u}(y,s)}{\partial y}\right]^2\end{aligned}\right)=0\\
&(1-p)\left(\frac{\partial^2 C}{\partial y^2}-\frac{\partial^2 C_0}{\partial y^2}\right)+\\
&p\left(\frac{\partial^2\bar{C}(y,s)}{\partial y^2}-\zeta\bar{C}(y,s)+SrSc\frac{\partial^2\bar{\theta}(y,s)}{\partial y^2}\right)=0
\end{aligned}\right\} \quad (41)$$

Assuming the solutions of Equations (41) are represented as a power series in the form defined by Equation (35), we arrive at:

$$\left.\begin{aligned}
&\bar{u}(y,s)=\sum_{n=0}^{\infty}p^n\bar{u}_n(y,s)=\bar{u}_0+p\bar{u}_1+p\bar{u}_2+\ldots\\
&\bar{\theta}(y,s)=\sum_{n=0}^{\infty}p^n\bar{\theta}_n(y,s)=\bar{\theta}_0+p\bar{\theta}_1+p\bar{\theta}_2+\ldots\\
&\bar{C}(y,s)=\sum_{n=0}^{\infty}p^n\bar{C}_n(y,s)=\bar{C}_0+p\bar{C}_1+p\bar{C}_2+\ldots
\end{aligned}\right\} \quad (42)$$

Substituting Equation (42) into Equation (41), we derive the following system in terms of the powers of the perturbation parameter.

$$p^0:\left\{\frac{\partial^2\bar{u}_0}{\partial y^2}=0,\frac{\partial^2\bar{\theta}_0}{\partial y^2}=0,\frac{\partial^2\bar{C}_0}{\partial y^2}=0\right. \quad (43)$$

The associated boundary conditions are expressed as:

$$\left.\begin{aligned}
&\bar{\theta}_0(-1)=\frac{1}{s+\lambda^2},\bar{u}_0(-1)=\frac{1}{s+\lambda^2},\\
&\bar{v}_0(-1)=\frac{1}{s+\lambda^2},\bar{C}_0(-1)=\frac{1}{s+\lambda^2}\\
&\bar{\theta}_0(1)\to 0,\qquad \bar{u}_0(1)\to 0,\bar{v}_0(1)\to 0,\\
&\bar{C}_0(1)\to 0
\end{aligned}\right\} \quad (44)$$

$$p^1:\begin{cases}\left(\begin{array}{l}\left(1+\lambda_2^{\beta}s^{\beta}\right)\dfrac{\partial^2\bar{u}_1}{\partial y^2}-\Lambda\bar{u}_0(y,s)-\\ \dfrac{h}{s}+\delta\bar{\theta}_0(y,s)+\gamma\bar{C}_0(y,s)+\dfrac{g(y)}{s}\end{array}\right)=0\\ \left(\begin{array}{l}K_1\dfrac{\partial^2\bar{\theta}_1(y,s)}{\partial y^2}-\eta\bar{\theta}_0(y,s)+\\ \dfrac{JHEc}{s}+Br\left(1+\lambda_2^{\beta}s^{\beta}\right)\left[\dfrac{\partial\bar{u}_0(y,s)}{\partial y}\right]^2\end{array}\right)=0....(45)\\ \left(\begin{array}{l}\dfrac{\partial^2\bar{C}_1(y,s)}{\partial y^2}-\zeta\bar{C}_0(y,s)+\\ SrSc\dfrac{\partial^2\bar{\theta}_0(y,s)}{\partial y^2}\end{array}\right)=0\end{cases}$$

Subject to the boundary conditions;

$$\left.\begin{array}{l}\bar{\theta}_1(-1)=\dfrac{1}{s+\lambda^2},\bar{u}_1(-1)=\dfrac{1}{s+\lambda^2},\\ \bar{v}_1(-1)=\dfrac{1}{s+\lambda^2},\bar{C}_2(-1)=\dfrac{1}{s+\lambda^2}\\ \bar{\theta}_1(1)\to 0,\qquad \bar{u}_1(1)\to 0,\\ \bar{v}_1(1)\to 0,\bar{C}_1(1)\to 0\end{array}\right\}\quad(46)$$

$$p^2:\begin{cases}\left(\begin{array}{l}\left(1+\lambda_2^{\beta}s^{\beta}\right)\dfrac{\partial^2\bar{u}_2}{\partial y^2}-\Lambda\bar{u}_1(y,s)\\ -\dfrac{h}{s}+\delta\bar{\theta}_1(y,s)+\gamma\bar{C}_1(y,s)+\dfrac{g(y)}{s}\end{array}\right)=0\\ \left(\begin{array}{l}K_1\dfrac{\partial^2\bar{\theta}_2(y,s)}{\partial y^2}-\eta\bar{\theta}_1(y,s)+\\ \dfrac{JHEc}{s}+Br\left(1+\lambda_2^{\beta}s^{\beta}\right)\left[\dfrac{\partial\bar{u}_1(y,s)}{\partial y}\right]^2\end{array}\right)=0...(47)\\ \left(\begin{array}{l}\dfrac{\partial^2\bar{C}_2(y,s)}{\partial y^2}-\zeta\bar{C}_1(y,s)+\\ SrSc\dfrac{\partial^2\bar{\theta}_1(y,s)}{\partial y^2}\end{array}\right)=0\end{cases}$$

Subject to the boundary conditions;

$$\left.\begin{array}{l}\bar{\theta}_2(-1)=\dfrac{1}{s+\lambda^2},\bar{u}_2(-1)=\dfrac{1}{s+\lambda^2},\\ \bar{v}_2(-1)=\dfrac{1}{s+\lambda^2},\bar{C}_2(-1)=\dfrac{1}{s+\lambda^2}\\ \bar{\theta}_2(1)\to 0,\qquad \bar{u}_2(1)\to 0,\\ \bar{v}_2(1)\to 0,\bar{C}_2(1)\to 0\end{array}\right\}\quad(48)$$

By solving Equations (43), (45), and (47) under the boundary conditions given in Equations (44), (46), and (88), the approximate solutions for the various orders are obtained as follows:

$$\left.\begin{array}{l}\bar{u}_0(y,s)=\dfrac{1}{s+\lambda^2}\left(1-\dfrac{y}{2}\right),\\ \bar{\theta}_0(y,s)=\dfrac{1}{s+\lambda^2}\left(1-\dfrac{y}{2}\right),\\ \bar{C}_0(y,s)=\dfrac{1}{s+\lambda^2}\left(1-\dfrac{y}{2}\right)\end{array}\right\}\quad(49)$$

$$\bar{u}_1(y,s)=\left(\frac{1}{1+\lambda_2^{\beta}s^{\beta}}\right)\left[\begin{array}{l}\Lambda\left(\dfrac{1}{s+\lambda^2}\left(\dfrac{y^2}{2}-\dfrac{y^3}{12}\right)+\right.\\ \dfrac{hy^2}{2s}-\delta\left(\dfrac{1}{s+\lambda^2}\left(\dfrac{y^2}{2}-\dfrac{y^3}{12}\right)\right.\\ -\gamma\left(\dfrac{1}{s+\lambda^2}\left(\dfrac{y^2}{2}-\dfrac{y^3}{12}\right)\right.\\ -\dfrac{1}{s(ke)^2}\left[\begin{array}{l}A\cosh(key)\\ +B\sinh(key)\end{array}\right]\\ -\dfrac{1}{2}\left[(A_1+B_1)y+(A_1+B_1)\right]\end{array}\right]\quad(50)$$

$$\bar{\theta}_1(y,s)=\left(\frac{1}{K_1}\right)\left[\begin{array}{l}\eta\left(\dfrac{1}{s+\lambda^2}\left(\dfrac{y^2}{2}-\dfrac{y^3}{12}\right)-\dfrac{JHEcy^2}{2s}-\right.\\ Br\left(1+\lambda_2^{\beta}s^{\beta}\right)\left[\dfrac{1}{s+\lambda^2}\right]^2y^2\\ -\dfrac{1}{2}\left[(M_1+M_2)y+(M_1+M_2)\right]\end{array}\right]\quad(51)$$

$$\bar{C}_1(y,s)=\left[\begin{array}{l}\zeta\left(\dfrac{1}{s+\lambda^2}\left(\dfrac{y^2}{2}-\dfrac{y^3}{12}\right)\right.\\ -\dfrac{1}{2}\left[(N_1+N_2)y+(N_1+N_2)\right]\end{array}\right]\quad(52)$$

The terms, $\bar{\theta}_n(y,s),\bar{u}_n(y,s)$ and $\bar{C}_n(y,s)$ when $n\geq 3$ are too large to be mentioned graphically. The two-term solution of Eq. (42), when $p\to 1$ is expressed as follows:

$$\left.\begin{aligned}\bar{u}(y,s) &= \bar{u}_0(y,s) + \bar{u}_1(y,s) + \ldots \\ \bar{\theta}(y,s) &= \bar{\theta}_0(y,s) + \bar{\theta}_1(y,s) + \ldots \\ \bar{C}(y,s) &= \bar{C}_0(y,s) + \bar{C}_1(y,s) + \ldots\end{aligned}\right\} \quad (53)$$

We utilized Gaby-Stefan's algorithm to compute the inverse Laplace Transform of Equation (53) and visually represented the results through simulations using MATCARD software.

5. Results and Discussion

This section provides a visual presentation of the findings, examining the behavior of the Atangana-Baleanu fractional Burgers' fluid model in relation to non-Newtonian blood flow in bifurcated arteries. The primary focus is on analyzing the effects of applied magnetics and electric fields, particularly in the context of tumor treatments. The graphical representations are designed to highlight key factors and their influence on the system. The key parameters under investigation include the Burgers' parameter, magnetic field strength, heat source parameter, Eckert number, Joule heating parameter, and radiation parameter.

$$\lambda = 1, M = 0.5, S = 0.5, R = 0.5, Ec = 0.5, JH = 0.5,$$
$$t = 0.3, \lambda_1 = 0.1, \lambda_2 = 0.07, Br = 0.5\lambda_3 = 0.7, \alpha = \beta = 0.7, R_{\xi} = 0.5, ke = 0.1, \Pr = 2.0, Sc = \omega = 0.5,$$
$$K = 0.5, \phi = 30^0, Sr = 0.5$$

These visual representations, along with the following discussions, aim to provide valuable insights into how each of these factors influences the complex dynamics of blood flow in bifurcated arteries, particularly in the context of tumor treatment.

5.1 Results of Velocity profile

In this section, we provided a visual presentation of the findings. This phase primarily investigates the behaviour of the Atangana-Baleanu time fractional derivative of Burgers' fluid in the context of non-Newtonian blood flow through bifurcated arteries. The graphical representations of these results are designed to shed light on various critical factors and their effects on the system.

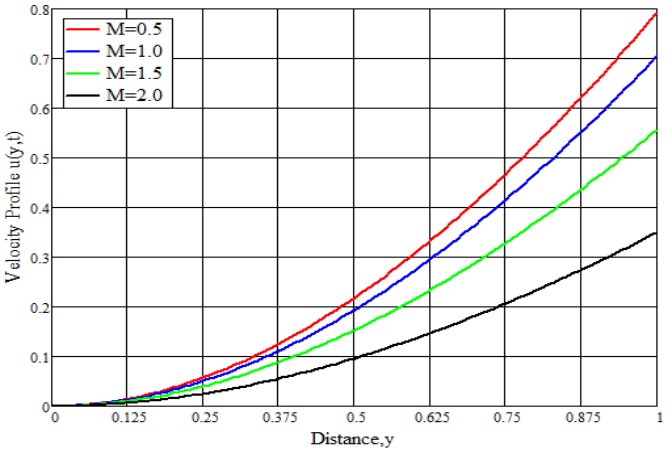

Figure 2: Velocity profile of Fractional Burgers fluid model with Magnetic Field Parameter

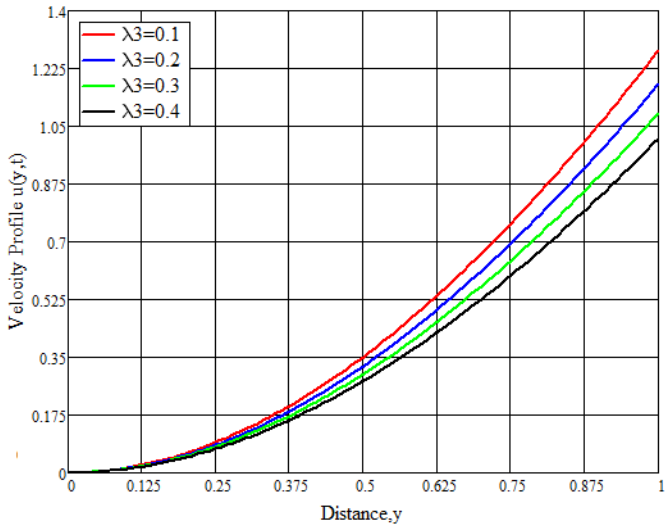

Figure 3: Velocity profile of Fractional Burgers fluid model with Burgers' Parameter

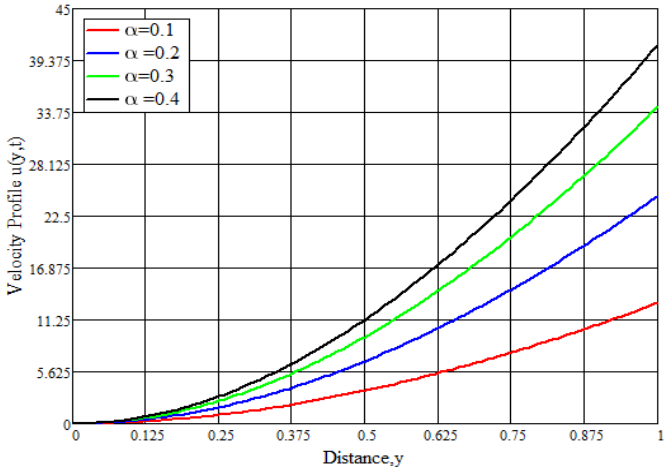

Figure 4: Velocity profile of Fractional Burgers fluid model with Fractional Parameter

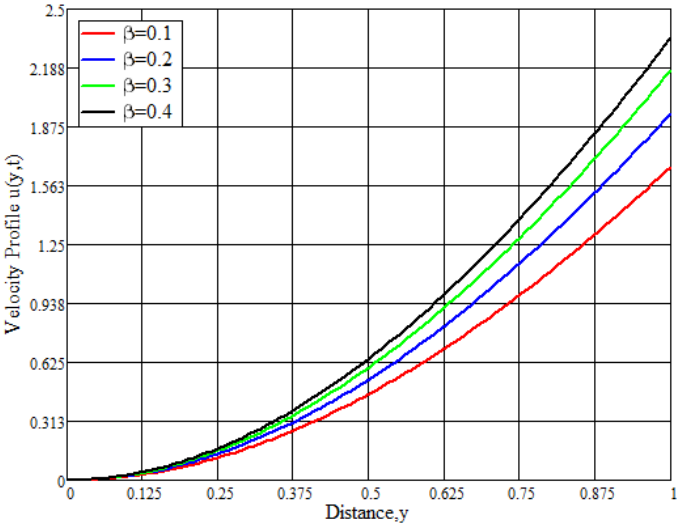

Figure 5: Velocity profile of Fractional Burgers fluid model with Fractional Parameter

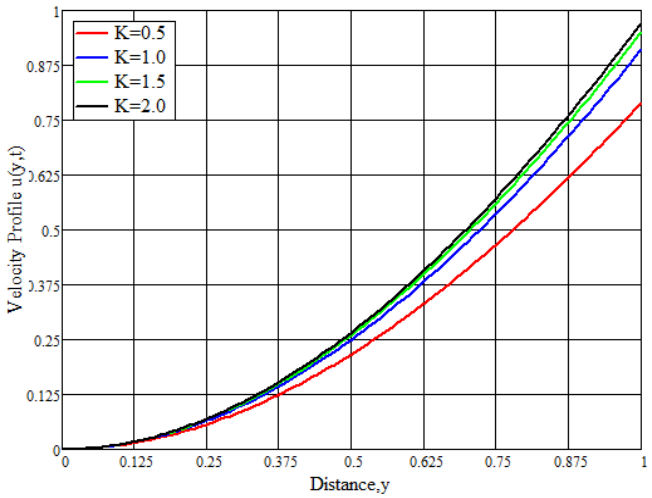

Figure 6: Velocity profile of Fractional Burgers fluid model with Porosity Parameter

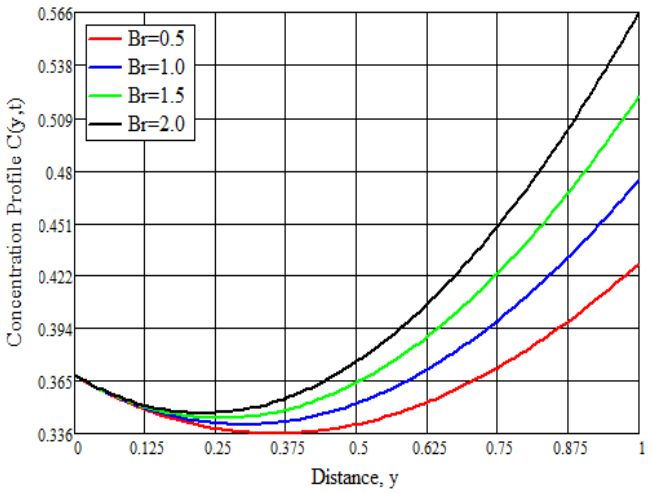

Figure 7: Concentration profile of Fractional Burgers fluid model with Brickman Number

Figure 2 examines how the magnetic field parameter affects the velocity of Burgers' fluid in bifurcated arteries. Increasing the magnetic field strength results in a notable decrease in fluid velocity, due to the Lorentz force acting against the flow**.** Figure 3: shows the impact of the Burgers' parameter on blood flow velocity. An increase in the Burgers' parameter which represents the viscoelastic properties of the fluid results in a reduction in velocity. This deceleration is more pronounced near the arterial wall, highlighting the fluid's viscoelastic resistance under deformation, which aligns with previous studies [3,4,5] on viscoelastic fluid dynamics in biological systems. In Figure**,** the fractional parameter α's effect on velocity is depicted. Higher values of α, representing fractional derivatives, lead to a more gradual change in flow dynamics. This parameter reflects memory effects in the fluid; thus, as α increases, the blood flow exhibits a smoother transition in velocity distribution.

Figure 5 explores the fractional parameter's role in controlling velocity. It demonstrates that as fractional derivative values increase, the velocity profile becomes more stable, suggesting a time-dependent behavior of blood flow in bifurcated arteries under various fractional orders, adding complexity to the viscoelastic flow model. Whereas Figure 6 shows how the porosity parameter influences velocity. Increased porosity reduces velocity, as porous arterial walls create additional resistance to blood flow. This result aligns with findings that porous media impede flow due to increased surface interaction**.**

5.2 The Concentration profile

In this part, we employ mathematical Modeling and analysis to visually represent and investigate numerical data on the concentration pattern of non-Newtonian blood flow in branched arteries. Our objective is to investigate how fractional parameters affect this concentration pattern, especially in relation to treating tumors. By using mathematical methods, we acquire important insights into the intricate dynamics of blood flow influenced by these critical factors. This research contributes significantly to the progress of medical science and treatment techniques.

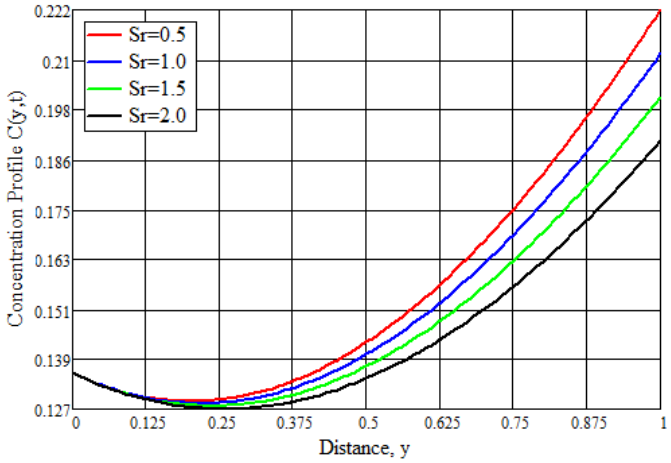

Figure 8: Concentration profile of Fractional Burgers fluid model with Soret Number

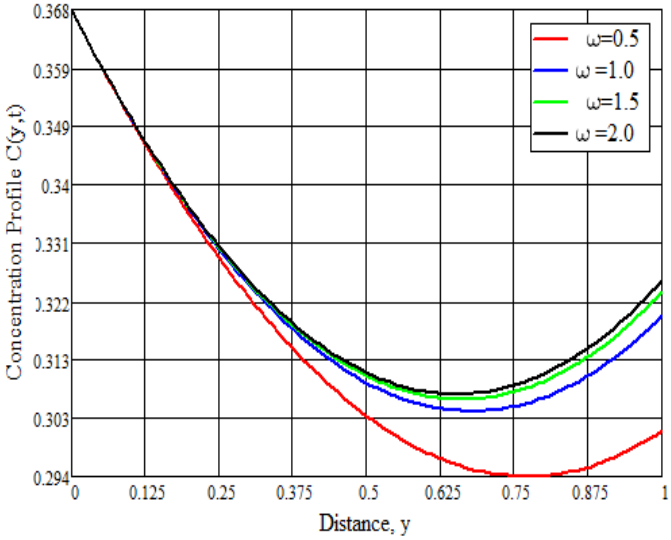

Figure 9: Concentration profile of Fractional Burgers fluid model with Chemical Reaction Parameter

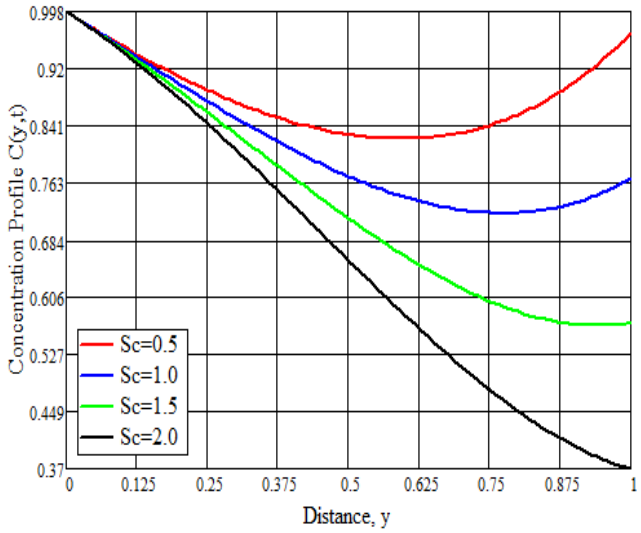

Figure 10: Concentration profile of Fractional Burgers fluid model with Schmidt Number

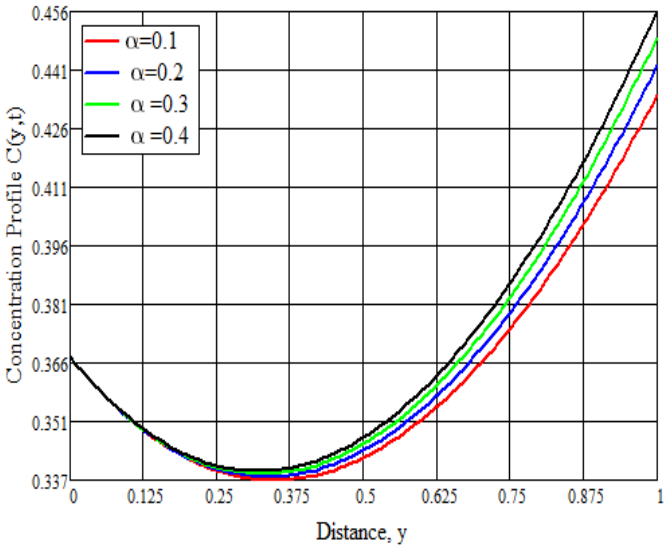

Figure 11: Concentration profile of Fractional Burgers fluid model with Fractional Parameter (Alpha)

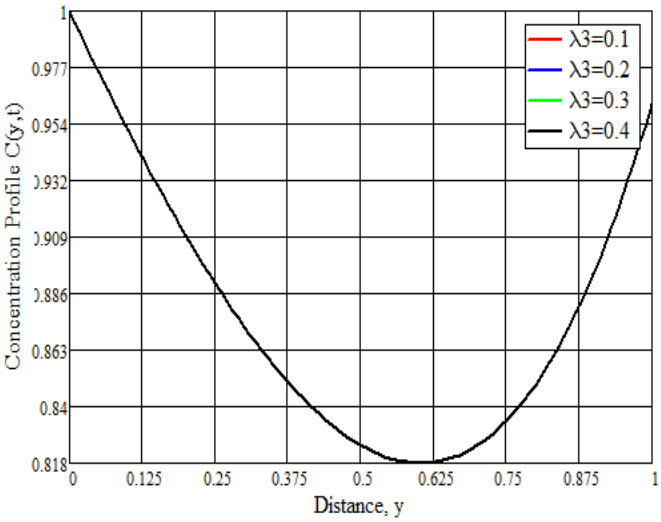

Figure 12: Concentration profile of Fractional Burgers fluid model with Burgers' Parameter

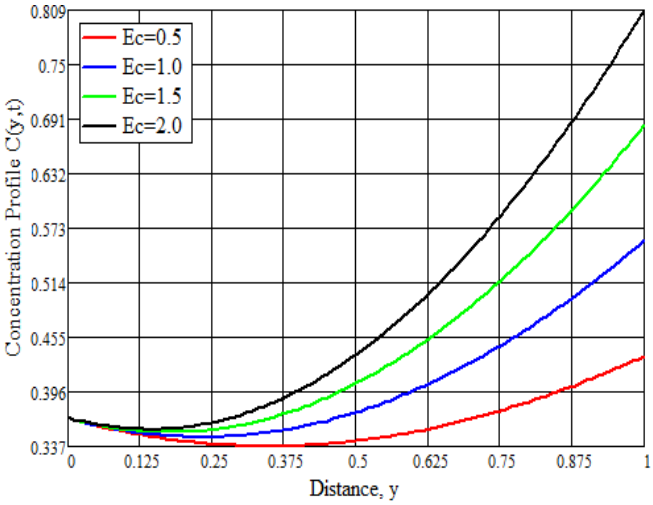

Figure 13: Concentration profile of Fractional Burgers fluid model with Eckert Number

Figure 7 illustrates the concentration profile as affected by the Brickman number, which relates to the fluid's molecular diffusivity. Higher values lead to a sharper concentration gradient, indicating enhanced molecular diffusion, which could be useful for drug delivery in medical treatments. In Figure 8**,** the Soret number's effect on concentration is shown here, with increased values leading to a higher concentration gradient. The Soret effect describes thermo-diffusion, where concentration increases in response to temperature gradients, aiding in targeted therapeutic delivery. Figure 9 displays the concentration profile influenced by chemical reaction rates. Higher reaction parameters reduce concentration in certain regions, suggesting that active biochemical reactions in blood flow, like those involved in tumor treatment, affect solute concentration. While Figure 10 shows the Schmidt number's effect on concentration. As the Schmidt number (a ratio of momentum to mass diffusivity) increases, diffusion is more restricted, resulting in a lower concentration spread. This behavior is essential for predicting solute dispersion in medical applications.

In Figure 11, the fractional parameter's impact on concentration distribution is demonstrated. Increasing the fractional parameter smooths out concentration gradients, indicating a more stabilized concentration profile, relevant to understanding long-term drug diffusion in arterial flows. Figure 12, illustrates how the Burgers' parameter affects concentration. Higher Burgers' values, representing greater viscoelastic resistance, tend to limit concentration, as fluid structure hinders diffusion. In Figure 13 the Eckert number's influence on concentration is shown here, indicating how energy dissipation affects diffusion rates. Higher Eckert values result in lower concentration, due to enhanced thermal effects and interaction with diffusion processes in the arterial wall.

5.3 The Temperature profile

In this section, we delve into the numerical findings that reveal the thermal properties of Burgers' fluid flow in bifurcated arteries. Our approach involves using detailed graphical representations to offer a comprehensive

understanding of the interplay among various influential variables. This segment primarily focuses on showcasing the significant effects of two crucial parameters: the Eckert number and the Joule heating parameter, on the dynamics of blood flow within this complex system.

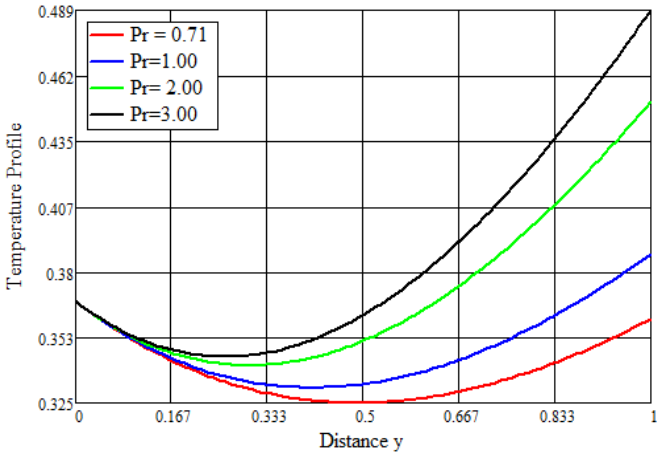

Figure 14: Temperature profile of Fractional Burgers fluid model with Prandtl number

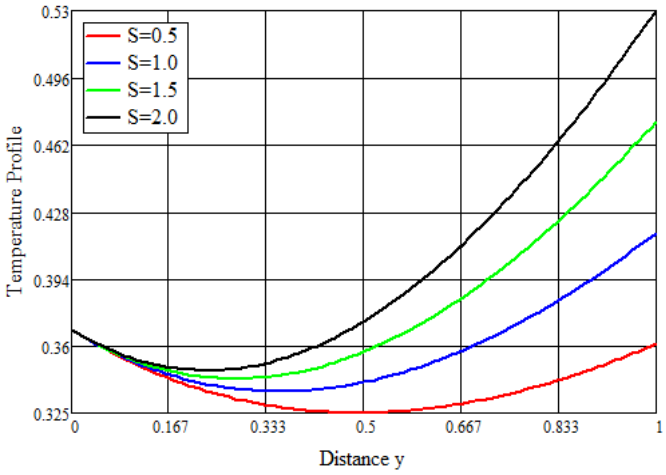

Figure 15: Temperature profile of Fractional Burgers fluid model with Heat source

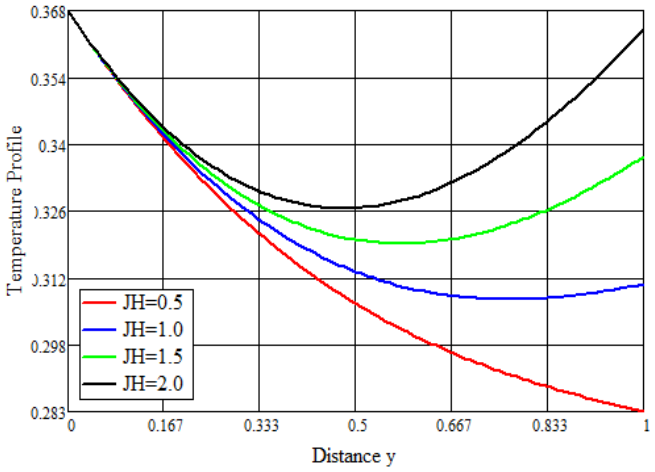

Figure 16: Temperature profile of Fractional Burgers fluid model with Joule heating Parameter

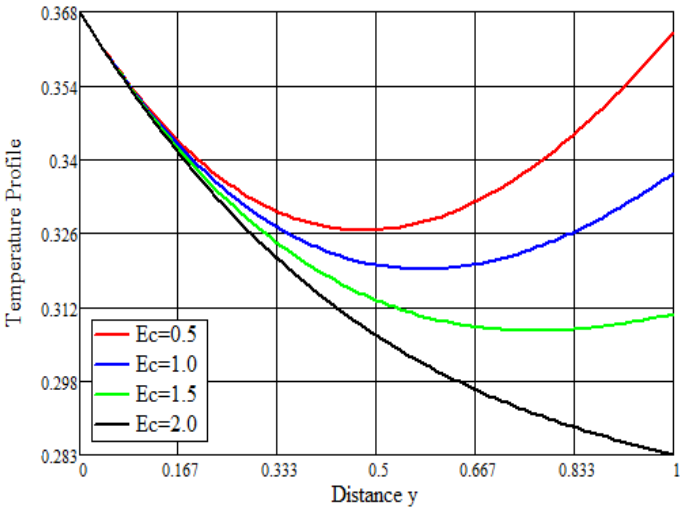

Figure 17: Temperature profile of Fractional Burgers fluid model with Eckert Number

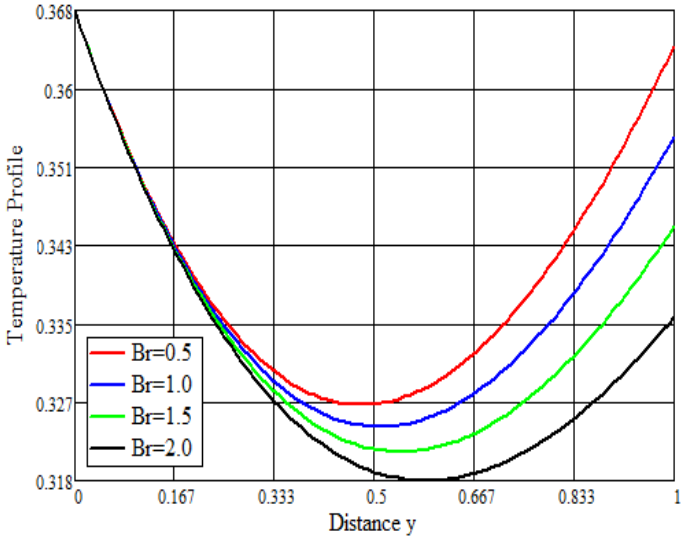

Figure 19: Temperature profile of Fractional Burgers fluid model with Brinkman Number

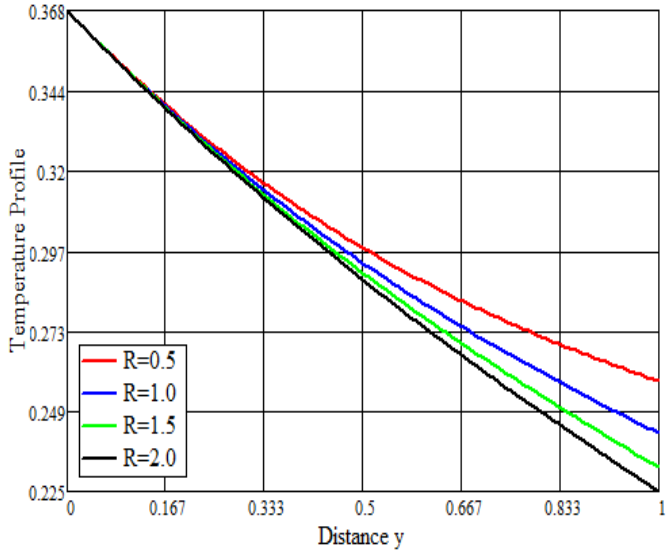

Figure 20: Temperature profile of Fractional Burgers fluid model with Radiation Parameter

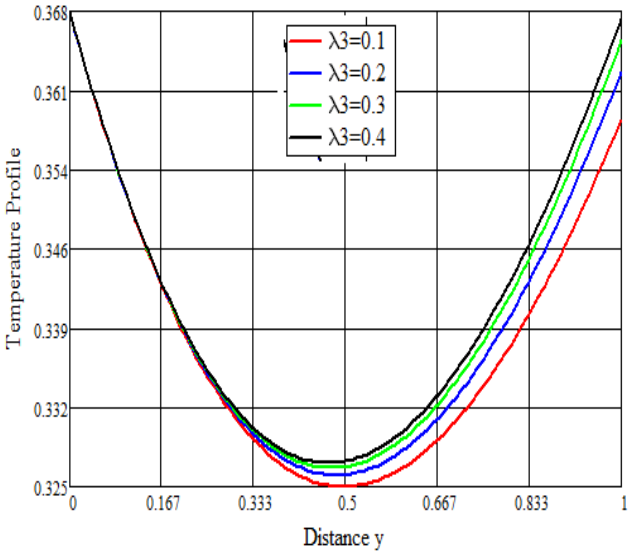

Figure 21: Temperature profile of Fractional Burgers fluid model with Burgers 'Parameter

Figure 14 illustrates the effect of the Prandtl number on temperature distribution. Higher Prandtl values, which represent the ratio of momentum diffusivity to thermal diffusivity, result in a steeper temperature gradient, indicating that heat transfer is dominated by viscous effects rather than conduction. Figure 15 demonstrates how the heat source parameter impacts the temperature profile. A higher heat source parameter increases the temperature, especially near the arterial walls, which could be useful in tumor hyperthermia treatments requiring localized heating. Figure 16 shows the effect of Joule heating, where electric currents within the blood raise the temperature. Increased Joule heating results in a steeper temperature rise, making it suitable for treatments needing controlled heating in specific areas. Figure 17 highlights the role of the Eckert number in temperature distribution. Higher Eckert values, representing kinetic energy dissipation, increase the temperature due to greater viscous dissipation in the fluid, consistent with non-Newtonian heating models for blood flow. Figure 18 illustrates the impact of the Brinkman number, which represents viscous heating relative to conduction. Higher Brinkman values result in greater temperature increases in high-shear areas, relevant for biomedical applications requiring precise temperature control. Figure 19 demonstrates the influence of the radiation parameter on temperature, with higher radiation values leading to elevated temperatures due to radiative heat transfer supplementing conductive and convective heat. This is important for treatments that require controlled energy absorption in biological tissues. Finally, Figure 20 examines how the Burgers' parameter affects the temperature profile, with higher values leading to reduced temperatures. The increased viscoelastic resistance limits heat dissipation, aligning with findings on non-Newtonian fluid systems' viscoelastic behavior.

6. Conclusion and Future Scope

This study presents a detailed analytical solution to the Burgers' fluid model for magnetohydrodynamic (MHD) blood flow through bifurcated arteries, incorporating the Atangana-Baleanu fractional derivative. The findings illustrate those parameters such as magnetic field strength, Burgers' parameter, Eckert number, and Joule heating influence blood flow, temperature, and concentration profiles significantly. These results are promising for enhancing biomedical applications, particularly in tumor treatment, by controlling blood flow and heat transfer within bifurcated arteries. The reduction in velocity with increasing magnetic field and viscoelasticity suggests that MHD effects can be instrumental in precision-targeting treatments. The interplay of these parameters offers insights into designing more efficient drug delivery systems and improving the accuracy of heat-based therapies.

Data Availability
Not applicable

Conflict of Interest
Authors declare that they do not have any conflict of interest.

Funding Source
No funding source exists.

Authors' Contributions
All authors reviewed and edited the manuscript and approved the final version of the manuscript.

Acknowledgements
The authors gratefully acknowledged the reviewers and the Editor in-chief for their comments and necessary suggestions.

Appendix

$$\Lambda = \left(\frac{s^{\alpha}(1+\lambda_1^{\alpha}s^{\alpha}+\lambda_3^{2\alpha}s^{2\alpha})}{s^{\alpha}(1-\alpha)+\alpha}\right)+(1+\lambda_1^{\alpha}s^{\alpha}+\lambda_3^{2\alpha}s^{2\alpha})M^2\sin^2\phi+\frac{(1+\lambda_1^{\alpha}s^{\alpha}+\lambda_3^{2\alpha}s^{2\alpha})}{K}$$

$$\delta = (1+\lambda_1^{\alpha}s^{\alpha}+\lambda_3^{2\alpha}s^{2\alpha})g\beta, \quad \gamma = (1+\lambda_1^{\alpha}s^{\alpha}+\lambda_3^{2\alpha}s^{2\alpha})g\beta'$$

$$K_1 = (1+\lambda_1^{\alpha}s^{\alpha}+\lambda_3^{2\alpha}s^{2\alpha})(\frac{1}{\tau\,\mathrm{Pr}}+R)$$

$$\eta = \left(\frac{s^{\alpha}(1+\lambda_1^{\alpha}s^{\alpha}+\lambda_3^{2\alpha}s^{2\alpha})}{s^{\alpha}(1-\alpha)+\alpha}\right)+(1+\lambda_1^{\alpha}s^{\alpha}+\lambda_3^{2\alpha}s^{2\alpha})(\frac{S}{\tau\,\mathrm{Pr}}+\delta_E)$$

$$\zeta = \left(\frac{s^{\alpha}}{s^{\alpha}(1-\alpha)+\alpha}\right)+Sc\omega$$

$$A_1 = \left(\frac{1+\lambda_2^{\beta}s^{\beta}}{s+\lambda^2}\right)-\frac{3}{2}\left(\frac{1}{s+\lambda^2}\right)-\frac{h}{2s}+\frac{3\delta}{2}\left(\frac{1}{s+\lambda^2}\right)+\frac{3\gamma}{2}\left(\frac{1}{s+\lambda^2}\right)+\frac{1}{s(ke)^2}[A\cosh ke+B\sinh ke]$$

$$B_1 = \frac{1}{2}\left(\frac{1}{s+\lambda^2}\right)-\frac{h}{2s}-\frac{\delta}{2}\left(\frac{1}{s+\lambda^2}\right)-\frac{\gamma}{2}\left(\frac{1}{s+\lambda^2}\right)+\frac{1}{s(ke)^2}[A\cosh ke+B\sinh ke]$$

$$M_1 = \frac{K_1}{s+\lambda^2}-\frac{3\eta}{2}\left(\frac{1}{s+\lambda^2}\right)+\frac{JHEc}{2s}+\frac{Br}{8}(1+\lambda_2^{\beta}s^{\beta})\left(\frac{1}{s+\lambda^2}\right)^2$$

$$M_1 = \frac{\eta}{2}\left(\frac{1}{s+\lambda^2}\right)+\frac{JHEc}{2s}+\frac{Br}{8}(1+\lambda_2^{\beta}s^{\beta})\left(\frac{1}{s+\lambda^2}\right)^2$$

$$N_1 = \left(\frac{1}{s+\lambda^2}\right)-\frac{3\zeta}{2}\left(\frac{1}{s+\lambda^2}\right)$$

$$N_2 = \frac{\zeta}{2}\left(\frac{1}{s+\lambda^2}\right)$$

References

[1] T. Hayat, M. Qasim, and Z. Abbas, "Peristaltic motion of a Burger's fluid in a porous medium with heat and mass transfer," *Int. J. Heat Mass Transfer*, vol. **54**, no. **19-20**, pp. **4305-4312, 2011**.

[2] M. Khan and I. Shahzadi, "Numerical study of MHD flow and heat transfer of Burgers' fluid over a stretching sheet," *Appl. Math. Comput.*, vol. **268**, pp. **459-469, 2015**.

[3] T. Hayat, T. Muhammad, and M. Farooq, "Magnetohydrodynamic oscillatory flow of Burgers' fluid in a porous medium with thermal radiation," *J. Mol. Liquids*, vol. **220**, pp**. 477-484, 2016**.

[4] D. G. Yakubu, M. G. Abdulhameed, G. T. Adamu, R. Roslan, A. Issakhov, and M. Rahini-Gorji Bakouri, "Towards the exact solutions of Burger's fluid flow through arteries with fractional time derivative, magnetic field and thermal radiation effects," *J. Process Mech. Eng.*, **2021**.

[5] A. Atangana and D. Baleanu, "New fractional derivative with non-local and non-singular kernel: Theory and application to heat transfer model," *Thermal Sci.*, vol. **21**, no. **2**, pp. **761-766, 2016.**

[6] J. A. Smith and B. R. Johnson, "Control of fractional order systems using Atangana-Baleanu fractional derivatives," *IEEE Trans. Control Syst.*, vol. **45**, no. **3**, pp. **789-802, 2022.**

[7] X. Chen and Y. Wang, "Analytical solutions of Atangana-Baleanu fractional differential equations in viscoelasticity," *J. Mater. Sci.*, vol. **35**, no. **7**, pp. **1585-1597, 2023.**

[8] I. A. Mirza, M. Abdulhameed, and S. Shafie, "Magnetohydrodynamic approach of non-Newtonian blood flow with magnetic particles in stenosed artery," *Appl. Math. Mech.*, vol. **38,** no. **3**, pp. **379-392, 2017**.

[9] D. Kumar, B. Satyanarayana, K. Rajesh, D. Narendra, and K. Sanjeev, "Application of heat source and chemical reaction in magnetohydrodynamic blood flow through permeable bifurcated arteries with inclined magnetic field in tumor treatments," *J. Result Appl. Math.*, vol. **10**, pp. **1-13, 2021**.

[10] A. Isah, A. Musa, D. G. Yakubu, G. T. Adamu, A. Mohammed, A. Baba, S. Kadas, and A. Mahmood, "The impact of heat source and chemical reaction on MHD blood flow through permeable bifurcated arteries with tilted magnetic field in tumor treatments," *Comput. Methods Biomech. Biomed. Eng.*, **2023**.

[11] A. Rauf and Y. Mahsud, "Electro-magneto-hydrodynamic flows of Burger fluids in cylindrical domains with time exponential memory," *J. Appl. Comput. Mech.*, vol. **5**, no. **4**, pp. **577-591, 2019**.

[12] M. Abdulhameed, G. T. Adamu, and D. G. Yakubu, "Modeling electro-osmotic flow and thermal transport of Caputo fractional Burgers' fluid through micro-channel," *J. Process Mech. Eng.*, **2021**.

[13] J. Escandon, E. Jimenez, O. Hernandez, O. Bautista, and F. Mendez, "Transient electroosmotic flow of Maxwell fluids in a slit microchannel with asymmetric zeta potentials," *Eur. J. Mech. B/Fluids*, vol. **53**, pp. **180-189, 2015.**

[14] J. H. He, "Homotopy perturbation method," *Comput. Math. Appl.*, vol. 37, no. 5, pp. **89-99, 1999.**

[15] J. H. He, "A new interpretation of the homotopy perturbation method," *Math. Comput. Modell.*, vol. **31**, no. 3, pp. **51-55, 2000**.

